HHS Public Access

Author manuscript

Cancer Res. Author manuscript; available in PMC 2020 March 15.

Published in final edited form as:

Cancer Res. 2019 September 15; 79(18): 4703–4714. doi:10.1158/0008-5472.CAN-19-0868.

Gene editing of α6 integrin inhibits muscle invasive networks and increases cell-cell biophysical properties in prostate cancer

Cynthia S. Rubenstein[1], **Jaime M.C. Gard**[1], **Mengdie Wang**[1], **Julie E. McGrath**[1], **Nadia Ingabire**[1], **James P. Hinton**[1], **Kendra D. Marr**[1], **Skyler J. Simpson**[1], **Raymond B. Nagle**[2], **Cindy K. Miranti**[1,3], **Noel A. Warfel**[3], **Joe G.N. Garcia**[5], **Hina Arif-Tiwari**[6], **Anne E. Cress**[1,2,3,4]

[1]Cancer Biology Research Program, University of Arizona Cancer Center, University of Arizona, Tucson, AZ 85724

[2]Dept. of Pathology, University of Arizona Cancer Center, University of Arizona, Tucson, AZ 85724

[3]Cellular and Molecular Medicine, University of Arizona Cancer Center, University of Arizona, Tucson, AZ 85724

[4]Radiation Oncology, University of Arizona Cancer Center, University of Arizona, Tucson, AZ 85724

[5]Dept. of Medicine, University of Arizona Cancer Center, University of Arizona, Tucson, AZ 85724

[6]Medical Imaging and the University of Arizona Cancer Center, University of Arizona, Tucson, AZ 85724

Abstract

Human prostate cancer (PCa) confined to the gland is indolent (low-risk) but tumors outside the capsule are aggressive (high-risk). Extracapsular extension requires invasion within and through a smooth muscle-structured environment. Since integrins respond to biomechanical cues, we used a gene editing approach to determine if a specific region of laminin-binding α6β1 integrin was required for smooth muscle invasion both in vitro and in vivo. Human tissue specimens showed PCa invasion through smooth muscle and tumor co-expression of α6 integrin and E-cadherin in a cell-cell location and α6 integrin in a cell-ECM distribution. PCa cells expressing α6 integrin (DU145 α6WT) produced a 3D invasive network on laminin-containing matrigel and invaded into smooth muscle both in vitro and in vivo. In contrast, cells without α6 integrin (DU145 α6KO) and cells expressing an integrin mutant (DU145 α6AA) did not produce invasive networks, could not invade muscle both in vitro and in vivo, and surprisingly formed 3D cohesive clusters. Using ECIS (electric cell-substrate impedance) testing, cohesive clusters had up to a thirty-fold increase in normalized resistance at 400Hz (cell-cell impedance) as compared to the DU145 α6WT cells. In contrast, measurements at 40,000 Hz (cell-ECM coverage) showed that DU145 α6AA cells were two-fold decreased in normalized resistance and were defective in restoring resistance after a 1uM S1P challenge as compared to the DU145 α6WT cells. The results suggest that gene editing of a

Corresponding Author: Anne E. Cress, University of Arizona Cancer Center, 1515 N. Campbell Ave., Tucson, AZ 85724. Phone: 520-626-7553; cress@email.arizona.edu.

COI Declaration: The authors declare no potential conflicts of interest.

specific α6 integrin extracellular region, not required for normal tissue function, can generate a new biophysical cancer phenotype unable to invade the muscle, presenting a new therapeutic strategy for metastasis prevention in PCa.

Keywords

α6p integrin; PCa; cohesive cluster phenotype; muscle invasion

Introduction

Recent advances in our understanding of the tumor microenvironment underscore the importance of biophysical properties of the tissue of origin and collective migration as defining features for metastasis (1,2). The nature of the extracellular matrix (ECM) material surrounding the tumor often determines how a tumor will migrate within and outside of the primary organ; there are multiple mechanisms that occur in 3D migration (3,4). The microenvironment of the human prostate is a simple glandular epithelium embedded in muscle and within the peripheral zone; a smooth muscle casing, known as the prostate capsule, defines the boundary of the gland (5). Lethal PCa escapes through the smooth muscle, along myelinated nerves (6,7), and disseminates via a hematogenous route to bone (8). These tumor microenvironments are structured tissue that depend, in part, upon a laminin-containing ECM (9,10). Anatomical and biophysical considerations point to dynamic collective migration as a likely mode of PCa invasion and metastasis through these varied ECM environments (11,12). The ECM environment can provide positive feedback and serve as a persistent migration cue for the transition to invasive cancer (13).

Because integrins reciprocally respond to biomechanical cues (14), we investigated the requirement for a tumor-specific laminin-binding integrin, called α6pβ1 integrin, to invade smooth muscle. For simplicity, α6β1 and α6pβ1 integrin are called α6 and α6p, respectively. The α6 integrin expression is a marker of aggressive clinical behavior in both human breast and PCa (15–18). The α6 integrin and urokinase plasminogen activator receptor (uPAR, CD87) functionally interact on the cell surface to produce a tumor specific α6p integrin missing the extracellular domain, via urokinase, in PCa cells (19–21). Amino acid residues R594 and R595, located in the “stalk” region of integrin α6, are required for the cleavage reaction (22). While both α6 integrin and uPAR (23–25) separately are associated with increased invasion and a malignant phenotype in several epithelial human cancers, the purpose of the current study was to use a Crispr/Cas9 gene editing approach to determine if invasion of prostate tumor cells through muscle was dependent upon production of the α6p integrin variant. Tumor cells expressing an uncleavable mutant α6 integrin (DU145 α6AA) were not invasive into smooth muscle and, unexpectedly, resulted in a biophysical phenotype with increased cell-cell adhesion and reduced cell-ECM biophysical properties. These data underscore an unexpected bioactivity of a specific α6 integrin extracellular region that is not required for normal tissue function to generate a new biomechanical phenotype in cancer cells that is unable to invade a smooth muscle barrier.

Materials and Methods

Cells, Antibodies and Reagents

DU145 cell line was obtained from the American Tissue Type Collection (ATCC, Manassas, VA). The cell line was cultured in Iscove's modified Dulbecco's medium (IMDM) from Mediatech (Manassas,VA) supplemented with 10% fetal bovine serum (FBS) Hyclone Laboratories (Novato, CA) and incubated at 37° in a 5% CO_2 humidified chamber. Non-enzymatic Cellstripper (CelGro, Manassas, VA) was used for cell harvesting. Antibodies used for immunofluorescence microscopy include: anti-α6 integrin (A6NT, (21)), anti-Desmin (Atlas Antibodies HPA018803), anti-E-Cadherin M168 (Abcam ab76055), anti-CK5/14 (KA2), anti-CK18 (Abcam EPR1626), and anti-FOXA1 (Abcam EPR10881). Antibodies used for flow cytometry include: anti-α6 integrin phycoerythrin (PE) conjugated GoH3 (eBioscience, San Diego, CA) and ADG3937 (Sekisui Diagnostics) mouse monoclonal antibody against uPAR. Alexa Fluor 488 (Invitrogen) secondary antibody was used for uPAR detection.

Genome editing

Homozygous knock-out cell line for ITGA6 gene (DU145 α6KO) and homozygous amino acid substitutions for ITGA6 R594A and R595A (DU145 α6AA) were created using CRISPR/Cas9 technologies in the University of Arizona Cancer Center (UACC) Genome Editing Facility. Colonies were screened by AA-specific PCR primer and agarose gel electrophoresis. Clones that were positive for AA amplification fragment internal to the targeted deletion were sent for sequencing. Parental PCa cells DU145 were transfected with Cas9 protein, crRNAs, and tracrRNA (Integrated DNA Technologies) using the Lipofectamine RNAiMAX reagent (Thermo Fisher Scientific). Two days after transfection, cutting efficiency was estimated based on DNA prepared from a portion of the transfected cell population using a T7 endonuclease assay (New England BioLabs) employing PCR primers flanking the predicted ligation-junction product. Single cells were deposited in ten 96-well plates by UACC Flow Cytometry Shared Resource. Colonies were expanded and screened by PCR and agarose gel electrophoresis. Clones that were negative for a fragment internal to the targeted deletion but positive for a ligation-junction fragment were potentially homozygous for the deletion. Absence of α6 integrin or presence of α6 integrin AA mutant was confirmed by flow cytometry and western blot analysis. All cells were authenticated by the University of Arizona Genetics Core and mycoplasma tested in 2019 by the University of Arizona Cancer Center Research Core Services.

Immunoprecipitation and immunoblot analysis

DU145 cells were lysed in CHAPS lysis buffer (50mM Tris-HCL, 110mM NaCl, 5mM EDTA,1% CHAPS) supplemented with complete mini protease inhibitor cocktail (Roche, Indianapolis, IN) and phosphatase inhibitor cocktails 2 and 3 (Sigma, St. Louis, MO). The cell lysate was pre-cleared with protein G sepharose beads (GE Healthcare, Little Chalfont, UK) for 1 hr before β1 was immunoprecipitated (IP) using the TS2/16 antibody (1:100) for 2 hrs at 4°C with continuous rotation, followed by the addition of G sepharose beads for 1 hr. The lysates were then washed twice in CHAPS buffer, spun down and boiled with PBS and NuPAGE LDS sample buffer (ThermoFisher Scientific, Waltham, MA). The samples

were then resolved using SDS-PAGE and immunoblot analysis using the α6 integrin antibody, AA6NT (1:15,000), and detected with an HRP conjugated anti-rabbit secondary (1:500).

For supplemental data, total cell lysate was prepared using radioimmunoprecipitation buffer ((RIPA) 50mM TRIS, 150 nM NaCl, 1% Triton X-100, 0.10% SDS, 1% deoxycholate) supplemented with complete mini protease inhibitor cocktail (Roche, Indianapolis, IN) and phosphatase inhibitor cocktails 2 and 3 (Sigma, St. Louis, MO). The samples were then resolved by SDS-PAGE and immunoblotting using AA6NT α6 integrin (1:10,000) specific antibody, anti-FAK (1:500, BD cat#610088) and anti-uPAR (1:1000, D7X2N, Cell Signaling Technology, Danvers, MA). The anti-GAPDH rabbit monoclonal antibody 14C10 (1:4000, Cell Signaling Technology Danvers, MA) and all primary antibodies were detected by appropriate HRP conjugated secondary antibodies (1:10,000). The proteins were then visualized using chemiluminescence (ECL Western Blotting Detection System, Amersham, Arlington Heights, IL). Membranes were then visualized utilizing a western blot imaging system (Syngene, Frederick, MD) and densitometry measurements performed using Image J.

Immunohistochemistry

Formalin-fixed paraffin embedded (FFPE) tissue sections (5 uM thickness) were baked at 65°C overnight, washed in xylene 3 times, 7 mins each, to remove paraffin, followed by passing through 100%, 75%, 50% isopropanol, and dd$H_2$0 for rehydration. Antigen retrieval was performed using EnVision FLEX target retrieval solution high pH (DAKO, DM828) buffer and heated at 97°C using decloaking chamber for 20 mins. Slides were washed in washing buffer (0.1 M TRIS-HCl, 0.3 M NaCl, 0.1% Tween 20, and 7.7 mM NaN_3, pH 7.6 at 25°C) followed by blocking buffer (5%(v/v) Normal Goat Serum, 0.1 M TRIS-HCl, and 0.15 M NaCl, pH 7.6 at 25°C) for 30 mins. Primary antibodies were diluted in blocking buffer and incubated at 4°C overnight in a humidified chamber. Slides were washed 3 times in wash buffer and incubated with secondary antibody and Hoechst 33342 (1:1,000; Invitrogen) for 30 mins to 1 hour at room temperature. Slides were washed 3 times in washing buffer and then mounted using ProLong® Diamond Antifade Mountant (Thermo Fisher Scientific, P36970) and stored in the dark at room temperature overnight to cure the mountant. Specimens were imaged using a DeltaVision Core system (GE Healthcare Bio-Sciences) equipped with an Olympus IX71 microscope, a 10X objective (NA 0.4), 60X objective (NA 1.42), and a cooled charge-coupled CoolSNAP HQ2 camera (Photometrics). Images were acquired with softWoRx v1.2 software (Applied Science). Image processing used Photoshop and analysis used Image J plot profile.

3D indirect immunofluorescence microscopy

For 3D indirect immunofluorescence microscopy, cells grown in 3D cultures were fixed in 2% paraformaldehyde (EM grade) freshly prepared in PBS for 20 mins at room temperature. After fixation, wells were rinsed once in PBS and permeabilized with 0.5% Triton X-100 in PBS at room temperature for 10 min. After permeabilization, cells were rinsed 3 times, 10 mins each, with PBS:glycine (100 mM), blocked with 10% (v/v) of goat serum (Sigma) in IF buffer (130 mM NaCl, 7 mM Na_2HPO_4, 3.5 mM NaH_2PO_4, 7.7 mM NaN_3, 0.1% BSA, 0.2% Triton X-100, 0.05% Tween-20) for 1 h at room temperature, and primary antibodies

were incubated in the same solution overnight at room temperature. Cells were then washed 3 times, 20 mins each, with IF buffer, and incubated with secondary antibodies for 1 hr at room temperature. Cells were next washed once with IF buffer for 20 mins, and twice with PBS followed by incubation with Hoechst 33342 (1:1,000; Invitrogen) for 15 mins. Cultures were mounted and imaged as above.

3D Invasion Networks

Phenol red free and growth factor reduced Matrigel (10.5 mg/ml protein containing laminin 111, Corning, Corning, NY cat# 356231) was thawed on ice overnight in 4°C. 50uL of Matrigel was added per well of 48-well plates and allowed to solidify for 15 mins at 37°C. DU145 cells were then harvested with Cellstripper (CelGro, Manassas, VA) and 80,000 cells per well were added on top of the Matrigel. Each well was then brought up to a total volume of 500uL with IMDM medium supplemented with 5% FBS. The 3D cultures were then incubated at 37° in a 5% CO_2 humidified chamber for up to 12 hrs.

Electric cell-substrate impedance sensing (ECIS)

Electrical properties of confluent or wounded epithelium were measured using electric ECIS as described previously (26). Cell adhesion measurements were based on changes in resistance/capacitance to current flow applied at different frequencies (Applied Biophysics, Troy, NY, USA). 96-well plate (Applied Biophysics,96W10idf PET) was coated with laminin at 4°C overnight, cells were inoculated at 125,000 cells per well in 200 mL in triplicates, and resistance/capacitance was measured at 400 and 40,000 Hz. Biophysical parameters for Supplemental Table 1 were determined by dose-response: [Agonist] vs. response—Variable slope model: Y=Bottom+(X$\hat{}$Hillslope)*(Top-Bottom)/(X^HillSlope + EC50^HillSlope) using GraphPad Prism 8.

Prostate Smooth Muscle Invasion Assay

Prostate smooth muscle cells (PrSMC, Lonza Cat #CC-2587), 40,000 per well, were placed into tissue culture transwell inserts (Corning, 8uM pore, 24-well plate, Cat#351152) that had been pre-coated with 50ug/ml of Collagen I. The smooth muscle layer formed for a minimum of one week. A differentiated layer of PrSMCs was detected either by direct observation or staining for desmin, an intermediate filament protein specific for differentiated smooth muscle. The prostate tumor cells (500,000 cells per well) were placed into the insert for the invasion assay for 16 hrs at 37°C. The upper chamber contained serum-free media while the lower chambers contained media with 10% v/v FBS. After the incubation, the inserts were washed in PBS and fixed using PBS containing 2% v/v para-formaldehyde for 15 mins, washed, and processed for immunofluorescence microscopy (IFM). IFM was used to discriminate between PrSMC (elongated DAPI stained nuclei) and the prostate tumor cells (GFP-labelled). Approximately 50 different field images of GFP positive cells on the underside of the insert were collected for each well and analyzed using Image J.

For mouse tumor xenograft smooth muscle assay, NOD-SCID mice (NOD.Cg-Prkdc^{scid} Il2rg^{tm1Wjl}/SzJ, Strain 005557, Jackson Labs) (5 mice per group) were injected IP with human tumor cells (1 x 10^7 cells) and tumor colonies were allowed to grow on the

undersurface of the diaphragm and within the peritoneal cavity for 8 weeks, as previously described (27). The collected diaphragm from each animal is fixed and embedded so that the tumor colony is oriented on top of the muscle and transverse sections will detect the tumor displacing the myoepithelium and tumor invasion into and within the smooth muscle layer. Approximately 4mm of diaphragm can be analyzed using this method.

The experimental mouse studies were reviewed and approved by the Institutional Animal Care and Use Committee (IACUC) as Protocol Number: 07-029. The protocol was conducted in accordance with all applicable federal and institutional policies, procedures and regulations, including the PHS Policy on Humane Care and Use of Laboratory Animals, USDA regulations (9 CFR Parts 1, 2, 3), the Federal Animal Welfare Act (7USC 2131 et. Seq.), the Guide for the Care and Use of Laboratory Animals, and all relevant institutional regulations and policies regarding animal care and use at the University of Arizona.

Results

Distribution of α6 integrin and α6p integrin variant in muscle-invasive human PCa.

The majority of human PCa on the cell surface expresses α6 integrin (CD49f) (27), an essential receptor for epithelial homeostasis and effective wound healing (28). In this study, we determined the distribution of α6 integrin within muscle-invasive PCa, using archived and de-identified radical prostatectomy specimens. The same tissue section was stained for E-cadherin and desmin (Fig.1A) or α6 integrin alone (Fig.1B) or E-cadherin and α6 integrin (Fig.1C). Higher power images of same areas were collected for E-cadherin and desmin (Fig.1D) or α6 integrin alone (Fig.1E) or E-cadherin and α6 integrin (Fig.1F). PCa glands maintained a high expression of E-cadherin (Fig.1A, D) and a stromal invasive pattern separating desmin-positive muscle fibrils (Fig.1D, white arrow). A serial section of the same case was used to determine the distribution of α6 integrin (Fig. 1B, E) in the tumor and as expected, α6 integrin was present on the tumor cell surface both between the cells and at their basal aspect (12).

Cancer glands express the α6β1 heterodimer in contrast to the α6 integrin expression in normal prostate glands within the basal cells due to the α6β4 heterodimer (29). A comparison of E-cadherin and α6 integrin distribution showed areas of co-localization in the tumor (Fig. 1C, F, yellow) in a cell-cell location. The distribution of α6 integrin alone was found at the cell-ECM location (Fig. 1F, white arrowhead) and E-cadherin alone was found at the cell-cell location (Fig. 1F, **). The α6 integrin was also in vessels (V), as expected (Fig. 1E, F) (28). A tissue section containing high grade PCa (Gleason sum score 7) expressing cytokeratin 8/18 and normal glands, expressing cytokeratin 5/14, within the same section (Supplemental Fig. 1A) was analyzed for Fox A1 (Supplemental Fig. 1B), E-cadherin and desmin (Supplemental Fig. 1C) and α6 integrin (Supplemental Fig. 1D) expression. Within the same section, a prominent feature of infiltrative prostate cancer was found as detected by mucicarmine staining for mucin production (Supplemental Fig. 1E, F). These observations indicate that the distribution of α6 integrin and E-cadherin expression persisted in higher grade aggressive PCa that contained infiltrative glandular mucinous adenocarcinoma networks (30) and infiltrative remnants of smooth muscle (Supplemental Fig. 1 A–F).

Conversion of invasive networks to cohesive clusters requires an uncleavable integrin.

Since α6 integrin was present on the tumor cell surfaces invading muscle (Fig. 1), we next used an established 3D *in vitro* model of epithelial tumor invasion into Matrigel (31) to determine the requirement for α6 integrin. The invasive networks generated by DU145 α6WT cells were confirmed to be dependent upon FAK and uPAR (Supplemental Fig. 2A,B,C), using a siRNA strategy as reported by others (32). We confirmed that the invasive networks contained the characteristic pericellular proteolysis and penetration of Matrigel as documented by histopathology (Supplemental Fig. 3A, B). The invasive networks expressed α6 integrin and E-cadherin (Supplemental Fig. 3C, D). The DU145 α6WT cells produced pericellular proteolysis, similar to that reported by others in colon and breast cancer cells (33). Previous work using site-directed mutagenesis identified amino acid residues R594 and R595, located in the “stalk” region of α6 integrin, as essential for cleavage of α6 integrin to generate the α6p integrin structural variant (Fig. 2A). The cleavage site is located on the extracellular region of the protein between the beta-barrel domain and the thigh domain (22).

We therefore used a Crispr gene editing approach to determine the requirement of α6 integrin cleavage on invasive PCa networks and tumor formation. The DU145 tumor cells expressing α6 integrin (DU145 α6WT) produced a 3D invasive network within 12 hours after seeding in Matrigel, which was not observed in DU145 cells without the α6 integrin gene (DU145 α6KO) (Fig. 2B). DU145 cells expressing the uncleavable α6 integrin (DU145 α6AA) also were unable to form complete invasive networks under the same conditions as compared to the cells without the α6 integrin gene (DU145 α6KO). Surprisingly, the DU145 α6AA cells formed dynamic cohesive clusters that were quantified by an increasing cluster size (Fig. 2B, D, open squares) (see also Supplemental Movies 1, 2). Both DU145 α6WT and DU145 α6AA cells had α6 integrin on the cell surface (Fig. 2C) and DU145 α6KO did not express α6 integrin, as expected (Fig. 2C). All three cell lines had comparable levels of the β1 integrin on their cell surfaces as observed by flow cytometry (Fig. 2C). The guide RNAs sequences and the exon positions for gene editing are found in Supplemental Fig. 4A and the similar tumor growth kinetics of the resulting cell lines are found in Supplemental Fig. 4B.

Immunoprecipitation studies of β1 integrin showed that both the DU145 α6WT cells and the DU145 α6AA cell lines contained heterodimers with full-length α6 integrin, and DU145 α6AA cells contained an uncleavable form of the integrin with no production of α6p integrin (Fig. 2D). Using video time-lapse microscopy to record the network formation every hour, we observed that the networks in DU145 α6WT cells increased in a time-dependent manner by 2- to 3-fold in the branching interval and the total loop area over a 12-hour incubation period (Fig. 2E). In contrast, both DU145 cells without the α6 integrin gene (DU145 α6KO) and DU145 cells expressing an uncleavable mutant (DU145 α6AA) did not produce invasive networks over the same period. Interestingly, both cell lines formed cohesive clusters of cells rather than invasive networks. The cohesive cluster average size in the DU145 α6AA cells increased hourly up to two-fold over the 12-hour period (Fig. 2E). In contrast, the DU145 α6WT cells did not increase in their average cluster size over the same 12-hour period (Fig. 2E).

Distribution of α6 and uPAR during network formation *in vitro*.

Since PCa tissue (Fig. 1) contained a co-distribution of α6 integrin and E-cadherin expression during muscle invasion, we next determined the distribution of α6 integrin and E-cadherin in the invasive networks made by the DU145 α6WT cells (Fig. 3 A, B) and within the DU145 α6AA (Fig. 3 C, D) cohesive clusters. The α6 integrin and E-cadherin in DU145 α6WT cells co-distributed in both invasive networks (Fig. 3A) and in DU145 α6AA cells in cohesive clusters (Fig. 3 C). The corresponding distribution maps of α6 integrin and E-cadherin in DU145 α6WT (Fig. 3B) and DU145 α6AA (Fig. 3D) were determined along an arbitrary image line running from one edge (a) of the network or cluster to the other (b) for 200-300 microns. The image grey values were compared to the position within the image. In the invasive networks, the majority of both α6 integrin and E-cadherin image signals were found at the edges and throughout the structure (Fig. 3B). In the cohesive clusters, the maximum uncleavable α6 integrin image signal (>180 units) was found within the central region of the cluster at 40-80 microns, as compared to E-cadherin, which was present throughout the structure (Fig. 3D).

We next determined the distribution of uPAR, which generates α6p integrin and pericellular proteolysis of the ECM and coordinates a multi-protein complex at the plasma membrane (21,24). The invasive networks generated by DU145 α6WT cells, expressed α6 integrin and uPAR in a co-incident pattern (Fig.4A, yellow) and α6 integrin alone was expressed on the edges of the networks (Fig. 4A, red). Cohesive clusters of DU145 α6AA cells were remarkably compact (Fig. 4B) compared to the DU145 α6WT invasive networks (Fig. 4A). The cohesive clusters contained actively dividing cells as detected by the presence of condensed chromosomes (Fig. 4B, inset, yellow arrow). The distribution of uPAR and α6 integrin in the DU145 α6AA cohesive clusters was centrally located (Fig. 4B) in a cell-cell distribution pattern (Fig. 4B', inset). Pixel mapping confirmed that the α6 integrin pixel values were greatest at the edges of the network compared to those within the invasive network (Fig. 4C, red line). In contrast, uPAR expression was uniform throughout the invasive network (Fig. 4C, green line). The pixel map confirmed the distribution of both α6 integrin and uPAR within the interstices of the clusters (Fig. 4D). Taken together, the data show that the cleavable α6 integrin (DU145 α6WT) is distributed in the invasive networks at a cell-cell and cell-ECM location. In contrast, the uncleavable form of the α6 integrin (DU145 α6AA), uPAR, and E-cadherin are localized primarily in a cell-cell location.

Cell-cell biophysical properties are increased in cells expressing the α6 integrin mutant.

The localization of the laminin-binding integrins, including α6 integrin, at cell-cell locations is common in early embryonic cells and early morphogenic or patterning events [reviewed in (34)]. Since the cell-cell phenotype was prominent (Fig.3) and our earlier work showed cell-cell protection from excessive mechanical stretch mediated by α6β4 integrin (35), we tested whether cell-cell and cell-ECM biophysical properties were altered in DU145 α6AA mutants or DU145 α6KO cells as compared to the DU145 α6WT cells. We used electric cell-substrate impedance sensing (ECIS) as this would provide a sensitive and quantifiable means to test both resistance with time of culture and test the restorative potential of the population following a challenge with sphingosine 1-phosphate (S1P), a bioactive

phospholipid. S1P is known to augment cell-cell barrier function in endothelial cells via α6 integrin (35).

The expression of uncleavable α6 integrin (DU145 α6AA) significantly increased cell-cell resistance every two hours with a linear increase (slope= 3.014), and the highest normalized resistance of 7.6 was measured at 70 hours (Fig. 5A, red line). In contrast, the cells without α6 integrin (DU145 α6KO) or expressing the cleavable α6 integrin (DU145 α6WT) both had a slower linear increase of cell-cell resistance properties over the entire 70-hour period (Fig. 5A, green and blue lines). After 70 hours, the normalized resistance measured at 400Hz in the DU145 α6AA population was approximately 7.5-fold higher than that observed within the DU145 α6WT or DU145 α6KO population. The predicted plateaus (Supplemental Table 1) were 33.62 for DU145 α6AA, 1.657 for DU145 α6WT, and 1.600 for DU145 α6KO population. Using the 1uM S1P challenge treatment at 24 hours, the DU145 α6AA population responded with a persistently increasing rate of cell-cell resistance (slope= 2.226, Supplemental Table 1) over the 70-hour period, but the predicted plateau was 13.17 compared to 33.62 in the untreated cells (Supplemental Table 1). Only a slight response was observed in the DU145 α6WT population (Fig. 5A, blue dashed line) since the predicted plateau (Supplemental Table 1) was 1.824 under the treatment conditions compared to the untreated value of 1.657. Taken together, these data indicated uncleavable α6 integrin expression (DU145 α6AA) conferred an increased cell-cell adhesion resistance during establishment of a 2D culture monolayer and regained resistance to maintain a cell-cell resistance that is at least ten-fold higher than the baseline predicted plateau (13.17 versus 1.657, Supplemental Table 1) in the cleavable integrin population (DU145 α6WT).

Our next step was to determine if cell-ECM coverage was distinct in the cell lines dependent upon α6 integrin status. The cell-ECM normalized resistance measured using 40,000Hz was monitored for 70 hours in both cell lines, with and without a 1uM S1P challenge (Fig. 5B). While all cell lines contained a time-dependent increase in resistance, the DU145 α6WT cells had a predicted plateau of 3.601, with a slope of 2.371, as compared to the DU145 α6KO cells, which had a predicted plateau of 2.700 and a slope of 3.165, and DU145 α6AA cells, which had a predicted plateau of 2.106 and a slope of 3.76 (Supplemental Table 1). The DU145 α6WT cells responded to S1P challenge by increasing the rate of resistance (slope = 4.304) up to 2-fold higher as compared to the untreated cells (slope = 2.371) (Fig. 5B and Supplemental Table 1). In contrast, the S1P challenge in DU145 α6AA cells resulted in a slight decrease of a predicted plateau from 2.106 to 1.811. Taken together, the data indicate that cells expressing the non-mutated integrin (DU145 α6WT) have an increased cell-ECM coverage (predicted plateaus of 3.601 vs 2.106) and a robust S1P response (predicted plateau of 2.876 vs 1.811) compared to the DU145 α6AA expressing cells. Both the predicted plateau of cell-ECM coverage under normal culture conditions and under the treatment response is compromised in the DU145 α6AA cells expressing the mutated uncleavable integrin.

Invasion advantage of α6p integrin, *in vitro* and *in vivo*.

Since invasive networks required production of the α6p integrin variant, the next step was to test the ability of the integrin invasive networks to invade through laminin-containing

Matrigel, a smooth muscle cell layer, or a collagen layer *in vitro* (Fig. 6). The DU145 α6WT cells invaded the laminin-containing Matrigel, smooth muscle layer, and collagen. The DU145 α6KO cells were unable to invade the laminin-containing Matrigel. In contrast, cells expressing the α6 integrin mutant (DU145 α6AA) were unable to invade any of the *in vitro* barriers tested, i.e., laminin-containing Matrigel, smooth muscle cell layer, or collagen.

DU145 cells readily produce tumors in male SCID mice, which enabled the testing of the invasive potential of the cell lines *in vivo*. Using an IP injection route, the tumors arising from all three cell lines were tested for their ability to form colonies on the undersurface of the diaphragm and invade into the smooth muscle. The diaphragm is one of the few anatomical structures where skeletal and smooth muscle co-exist (27). The smooth muscle surface of the diaphragm with the accompanying endothelial lining is an ideal and physiologically relevant model for testing smooth muscle invasion occurring during PCa escape from the gland. All cell lines produced xenograft tumors that increased in volume over an 8-week period (Supplemental Fig. 3B). At the end of 8 weeks, the tumors were analyzed for angulated muscle invasive characteristics. All tumors were proliferative as judged by the appearance of mitotic cells within the tumors, and none of the tumors were necrotic. The DU145 α6WT tumors were able to invade the muscle (Fig. 7A) as compared to no or little invasion in the DU145 α6KO or DU145 α6AA mutant tumors (Fig. 7B, C). DU145 α6WT tumors resulted in approximately 18 invasion sites along the 4mm stretch of diaphragm with a maximum depth within the muscle of approximately 100 units (Fig. 7D). In contrast, the mice harboring DU145 α6KO or DU145 α6AA mutant tumors had less than five invasion sites and DU145 α6AA mutant tumors only invaded superficially into the muscle (Fig. 7D). Interestingly, all cell lines, independent of the α6 integrin status, were able to invade into the pancreas, an organ accessible by IP injection (Supplemental Fig. 5A, B, C).

Discussion

The human prostate is a simple glandular epithelium embedded in muscle and within the peripheral zone of the gland; a smooth muscle casing known as the prostate capsule defines the boundary of the gland (5). Aggressive PCa escapes through the smooth muscle, along myelinated nerves (6,7), and disseminates via a hematogenous route to bone (8). These tumor microenvironments are structured tissue that depend, in part, upon a laminin-containing ECM (9,10,36,37).

In previous work, we discovered human prostate tumor phenotypes based on differential laminin-binding integrin membrane expression in human tissue specimens (38). The predominant expression of laminin-binding integrins in PCa is the α6 integrin (CD49f), a known adhesion and signaling receptor for prostate epithelial stem cells (39,40). The current work tested the requirement of a tumor variant called α6p integrin to form invasive networks, invade into and through smooth muscle *in vitro*, and invade through muscle as a mouse xenograft tumor. While the need for α6 integrin for invasive network formation was previously reported in other cell types (41,42), the requirement of α6p integrin in forming invasion networks or invading into muscle was unknown. Our previous work showed that PCa progression and migration can be significantly delayed by blocking α6pβ1 production

either by genetic silencing or pharmacological strategies (21,43) and predicted the importance of the integrin cleavage site. A limitation of the previous work was that the methods did not allow for complete and stable elimination of the endogenous α6 integrin expression. Therefore, we used a Crispr/Cas9 method to eliminate the endogenous ITGA6 gene or alter ITGA6 gene to contain AA substitution mutations, eliminating the cleavage site. The use of gene editing approaches has the potential to generate off target effects, depending upon the target gene and the surrounding sequences (44). In our study, we generated at least three cell clones for each homozygous knockout that maintained the normal expression and surface expression of the other laminin binding integrins.

In the current work, α6 integrin mutant cells (DU145 α6AA) exclusively expressed an uncleavable α6 integrin and this resulted in the inability of the tumor cells to form invasive networks. Surprisingly, the tumor cells organized into cohesive clusters of cells with a dramatic increase in a cell-cell adhesion phenotype. The increased cell-cell adhesion phenotype in DU145 α6AA cells was functional as the cell-cell biophysical properties were dramatically increased as compared to those in DU145 α6WT or DU145 α6KO cells. The DU145 α6AA cells were responsive to a membrane disruptive challenge. We note also that the cohesive clusters have increased cell-cell interactions at the apparent expense of the cell–ECM coverage. The existence of the cohesive cluster phenotype in PCa specimens has been observed previously (12). Although the cohesive cluster phenotype can significantly slow tumor progression (43), it is dependent upon β1 integrin function and can provide resistance to chemotherapeutic and radiotherapeutic approaches by a variety of mechanisms (45,46). It remains to be determined if the cohesive cluster phenotype that blocks invasion here may result in tumors that are more resistant to chemotherapeutic agents. If this occurs, interrupting β1 integrin function may provide a strategy to increase local control of PCa.

As expected, the DU145 α6AA cells will phenocopy the DU145 α6KO cells by forming clusters, making no networks and no invasion into the smooth muscle of a mouse. Unexpectedly, the DU145 α6AA, in comparison to the DU145 α6KO cells, have a gain of phenotype with an increased cell-cell adhesion interaction (Figs. 3 and 5). This observation raises the possibility that alteration of the α6 integrin extracellular domain that is independent of ECM adhesion, may trigger cell-cell adhesion interactions. We note that a cross-talk between α6 integrin and E-cadherin occurs in early embryonic development (34). The potential of a specific extracellular domain of α6 integrin to alter cell-cell membrane interactions is also consistent with the principle of self-organization (47), a fundamental basis for evolution and natural selection. Further, we note that the co-distribution of uPAR and the modification of α6 integrin extracellular domain would influence membrane shape similar to the reported coupling of curved membrane proteins and cytoskeletal forces to produce dynamical shapes (48).

The DU145 α6AA strong phenotype (i.e., non-invasive and cell-cell clusters) is consistent with our previous findings that the blockage of α6 integrin cleavage by an exogenous supply of the J8H antibody, results in a dominant negative phenotype of invasion in the presence of the endogenous α6 integrin (21). Since both the DU145 α6WT and DU145 α6AA cells express α6 integrin with the domain to interact with uPAR, muscle invasive cancers contain elevated levels of uPAR expression (49), and membrane localization of uPAR regulates its

function (50), we speculate that the integrin mutation is a candidate to effectively regulate the uPAR-dependent process of smooth muscle invasion of PCa. Our previous studies have shown that uPA is a serine protease specifically responsible for generating the α6p integrin. The evidence includes the use of specific inhibitors, siRNA for uPA, uPAR, and the lack of a requirement for cationic co-factors needed for other general classes of proteases, such as kallikrein, metalloproteases or lysosomal proteases (51). It should be noted that while exogenously supplied proteases such as trypsin can generate α6p *in vitro*, the concentration and specific activity of the enzyme is far more than what is possible under physiologically relevant conditions.

It is remarkable that the α6 integrin mutation (R594A, R595A) which creates a gain of the cell-cell phenotype, occurs in the extracellular "stalk" region of the molecule. Previous work has focused either on the extracellular adhesion domains or the cytoplasmic signaling domains as regions responsible for integrins as bidirectional signaling machines. The data here suggests that altering other regions within the molecule may trigger changes in cell phenotype; a new consideration since most anti-integrin cancer therapeutic agents are created to antagonize extracellular domains for integrin adhesion or signaling functions that are also required for normal tissue function (52,53). New methods for predictable and precise Crispr genome editing in human cancers (54) or muscle-specific secretion of the J8H antibody (which blocks α6p production) as a novel DNA synthetic vaccine (55), may offer new strategies to block PCa-specific smooth muscle invasion and extracapsular extension.

Supplementary Material

Refer to Web version on PubMed Central for supplementary material.

Acknowledgements

We acknowledge staff support of the Tissue Acquisition and Cellular/Molecular Analysis Resource, the Experimental Mouse Shared Service and the Genome Editing Facility at the University of Arizona Cancer Center, without which this work could not have been done. We thank William Harryman for editorial services and manuscript submission. We acknowledge all the funding sources that made the work possible, including NIH-NCI RO1CA159406 (to AE Cress), NIH-NCI T32CA009213 (to AE Cress), NIH-NHLBI P01 HL126609, (to JGN Garcia, Project 3 (AE Cress)), NCI-P30 CA 23074, ACS-IRG (H Arif-Tiwari), the MARC program (T34GM08718) (N Ingabire), support to M Wang from the Tim and Diane Bowden Fellowship in Cancer Biology and an ARCS Foundation Award to KD Marr.

Financial Support: Research was supported in part by NIH-NCI RO1CA159406 (to A.E.C), NIH-NCI T32CA009213 (to A.E.C.), NIH-NHLBI P01 HL126609, (to J.G.N.G, Project 3 (A.E.C)), NCI-P30 CA 23074, ACS-IRG (H.T.), the MARC program (T34GM08718) (NI), support to M.W. from the Tim and Diane Bowden Fellowship in Cancer Biology and an ARCS Foundation Award to K.D.M.

References

1. Haeger A, Wolf K, Zegers MM, Friedl P. Collective cell migration: guidance principles and hierarchies. Trends Cell Biol 2015;25(9):556–66. [PubMed: 26137890]
2. Pickup MW, Mouw JK, Weaver VM. The extracellular matrix modulates the hallmarks of cancer. EMBO Rep 2014;15(12):1243–53. [PubMed: 25381661]
3. Petrie RJ, Yamada KM. Multiple mechanisms of 3D migration: the origins of plasticity. Curr Opin Cell Biol 2016;42:7–12. [PubMed: 27082869]

4. Neumann NM, Perrone MC, Veldhuis JH, Huebner RJ, Zhan H, Devreotes PN, et al. Coordination of Receptor Tyrosine Kinase Signaling and Interfacial Tension Dynamics Drives Radial Intercalation and Tube Elongation. Dev Cell 2018;45(1):67–82 e6. [PubMed: 29634937]
5. Petkova N, Hennenlotter J, Sobiesiak M, Todenhofer T, Scharpf M, Stenzl A, et al. Surface CD24 distinguishes between low differentiated and transit-amplifying cells in the basal layer of human prostate. Prostate 2013;73(14):1576–90. [PubMed: 23836489]
6. Powell MS, Li R, Dai H, Sayeeduddin M, Wheeler TM, Ayala GE. Neuroanatomy of the normal prostate. Prostate 2005;65(1):52–7. [PubMed: 15806576]
7. Sroka IC, Anderson TA, McDaniel KM, Nagle RB, Gretzer MB, Cress AE. The laminin binding integrin alpha6beta1 in prostate cancer perineural invasion. J Cell Physiol 2010;224(2):283–8. [PubMed: 20432448]
8. Coleman RE. Clinical features of metastatic bone disease and risk of skeletal morbidity. Clin Cancer Res 2006;12(20 Pt 2):6243s–49s. [PubMed: 17062708]
9. Schwalenberg T, Neuhaus J, Liatsikos E, Winkler M, Loffler S, Stolzenburg JU. Neuroanatomy of the male pelvis in respect to radical prostatectomy including three-dimensional visualization. BJU Int 2010;105(1):21–7. [PubMed: 19549118]
10. Sroka IC, Chopra H, Das L, Gard JM, Nagle RB, Cress AE. Schwann Cells Increase Prostate and Pancreatic Tumor Cell Invasion Using Laminin Binding A6 Integrin. J Cell Biochem 2016;117(2): 491–9. [PubMed: 26239765]
11. Nagle RB, Cress AE. Metastasis Update: Human Prostate Carcinoma Invasion via Tubulogenesis. Prostate Cancer 2011;2011:249290. [PubMed: 21949592]
12. Harryman WL, Hinton JP, Rubenstein CP, Singh P, Nagle RB, Parker SJ, et al. The Cohesive Metastasis Phenotype in Human Prostate Cancer. Biochim Biophys Acta 2016;1866(2):221–31. [PubMed: 27678419]
13. Kim DH, Ewald AJ, Park J, Kshitiz, Kwak M, Gray RS, et al. Biomechanical interplay between anisotropic re-organization of cells and the surrounding matrix underlies transition to invasive cancer spread. Sci Rep 2018;8(1):14210. [PubMed: 30242256]
14. Sun Z, Guo SS, Fassler R. Integrin-mediated mechanotransduction. J Cell Biol 2016;215(4):445–56. [PubMed: 27872252]
15. Davidson B, Konstantinovsky S, Nielsen S, Dong HP, Berner A, Vyberg M, et al. Altered expression of metastasis-associated and regulatory molecules in effusions from breast cancer patients: a novel model for tumor progression. Clin Cancer Res 2004;10(21):7335–46. [PubMed: 15534110]
16. Friedrichs K, Ruiz P, Franke F, Gille I, Terpe HJ, Imhof BA. High expression level of alpha 6 integrin in human breast carcinoma is correlated with reduced survival. Cancer Res 1995;55(4): 901–6. [PubMed: 7850807]
17. Ricci E, Mattei E, Dumontet C, Eaton CL, Hamdy F, van der Pluije G, et al. Increased expression of putative cancer stem cell markers in the bone marrow of prostate cancer patients is associated with bone metastasis progression. Prostate 2013;73(16):1738–46. [PubMed: 24115186]
18. Tagliabue E, Ghirelli C, Squicciarini P, Aiello P, Colnaghi MI, Menard S. Prognostic value of alpha 6 beta 4 integrin expression in breast carcinomas is affected by laminin production from tumor cells. Clin Cancer Res 1998;4(2):407–10. [PubMed: 9516929]
19. Davis TL, Rabinovitz I, Futscher BW, Schnolzer M, Burger F, Liu Y, et al. Identification of a novel structural variant of the alpha 6 integrin. J Biol Chem 2001;276(28):26099–106. [PubMed: 11359780]
20. Demetriou MC, Pennington ME, Nagle RB, Cress AE. Extracellular alpha 6 integrin cleavage by urokinase-type plasminogen activator in human prostate cancer. Exp Cell Res 2004;294(2):550–8. [PubMed: 15023541]
21. Ports MO, Nagle RB, Pond GD, Cress AE. Extracellular engagement of alpha6 integrin inhibited urokinase-type plasminogen activator-mediated cleavage and delayed human prostate bone metastasis. Cancer Res 2009;69(12):5007–14. [PubMed: 19491258]
22. Pawar SC, Demetriou MC, Nagle RB, Bowden GT, Cress AE. Integrin alpha6 cleavage: a novel modification to modulate cell migration. Exp Cell Res 2007;313(6):1080–9. [PubMed: 17303120]

23. Mazar AP. Urokinase plasminogen activator receptor choreographs multiple ligand interactions: implications for tumor progression and therapy. Clin Cancer Res 2008;14(18):5649–55. [PubMed: 18794071]
24. Blasi F, Verde P. Urokinase-dependent cell surface proteolysis and cancer. Semin Cancer Biol 1990;1(2):117–26. [PubMed: 2151734]
25. Sier CF, Stephens R, Bizik J, Mariani A, Bassan M, Pedersen N, et al. The level of urokinase-type plasminogen activator receptor is increased in serum of ovarian cancer patients. Cancer Res 1998;58(9):1843–9. [PubMed: 9581823]
26. Wegener J, Keese CR, Giaever I. Electric cell-substrate impedance sensing (ECIS) as a noninvasive means to monitor the kinetics of cell spreading to artificial surfaces. Exp Cell Res 2000;259(1): 158–66. [PubMed: 10942588]
27. McCandless J, Cress A, Rabinovitz I, Payne C, Bowden G, Knox J, et al. A human xenograft model for testing early events of epithelial neoplastic invasion. International journal of oncology 1997;10(2):279–85. [PubMed: 21533373]
28. Hogervorst F, Admiraal LG, Niessen C, Kuikman I, Janssen H, Daams H, et al. Biochemical characterization and tissue distribution of the A and B variants of the integrin alpha 6 subunit. J Cell Biol 1993;121(1):179–91. [PubMed: 7681434]
29. Davis TL, Cress AE, Dalkin BL, Nagle RB. Unique expression pattern of the alpha6beta4 integrin and laminin-5 in human prostate carcinoma. Prostate 2001;46(3):240–8. [PubMed: 11170153]
30. Gordetsky J, Epstein J. Grading of prostatic adenocarcinoma: current state and prognostic implications. Diagnostic pathology 2016;11:25. [PubMed: 26956509]
31. Sameni M, Cavallo-Medved D, Franco OE, Chalasani A, Ji K, Aggarwal N, et al. Pathomimetic avatars reveal divergent roles of microenvironment in invasive transition of ductal carcinoma in situ. Breast cancer research : BCR 2017;19(1):56. [PubMed: 28506312]
32. Casar B, Rimann I, Kato H, Shattil SJ, Quigley JP, Deryugina EI. In vivo cleaved CDCP1 promotes early tumor dissemination via complexing with activated beta1 integrin and induction of FAK/PI3K/Akt motility signaling. Oncogene 2014;33(2):255–68. [PubMed: 23208492]
33. Botkjaer KA, Deryugina EI, Dupont DM, Gardsvoll H, Bekes EM, Thuesen CK, et al. Targeting tumor cell invasion and dissemination in vivo by an aptamer that inhibits urokinase-type plasminogen activator through a novel multifunctional mechanism. Molecular cancer research : MCR 2012;10(12):1532–43. [PubMed: 23038812]
34. Bulgakova NA, Klapholz B, Brown NH. Cell adhesion in Drosophila: versatility of cadherin and integrin complexes during development. Curr Opin Cell Biol 2012;24(5):702–12. [PubMed: 22938782]
35. Chen W, Epshtein Y, Ni X, Dull RO, Cress AE, Garcia JG, et al. Role of Integrin beta4 in Lung Endothelial Cell Inflammatory Responses to Mechanical Stress. Sci Rep 2015;5:16529. [PubMed: 26572585]
36. Hedin U, Bottger BA, Forsberg E, Johansson S, Thyberg J. Diverse effects of fibronectin and laminin on phenotypic properties of cultured arterial smooth muscle cells. J Cell Biol 1988;107(1): 307–19. [PubMed: 2455726]
37. Thyberg J, Blomgren K, Roy J, Tran PK, Hedin U. Phenotypic modulation of smooth muscle cells after arterial injury is associated with changes in the distribution of laminin and fibronectin. J Histochem Cytochem 1997;45(6):837–46. [PubMed: 9199669]
38. Schmelz M, Cress AE, Scott KM, Burger F, Cui H, Sallam K, et al. Different phenotypes in human prostate cancer: alpha6 or alpha3 integrin in cell-extracellular adhesion sites. Neoplasia 2002;4(3): 243–54. [PubMed: 11988844]
39. Schmelz M, Moll R, Hesse U, Prasad AR, Gandolfi JA, Hasan SR, et al. Identification of a stem cell candidate in the normal human prostate gland. European journal of cell biology 2005;84(2–3): 341–54. [PubMed: 15819412]
40. Lawson DA, Zong Y, Memarzadeh S, Xin L, Huang J, Witte ON. Basal epithelial stem cells are efficient targets for prostate cancer initiation. Proceedings of the National Academy of Sciences of the United States of America 2010;107(6):2610–5. [PubMed: 20133806]
41. Smadja DM, Bieche I, Helley D, Laurendeau I, Simonin G, Muller L, et al. Increased VEGFR2 expression during human late endothelial progenitor cells expansion enhances in vitro

angiogenesis with up-regulation of integrin alpha(6). Journal of cellular and molecular medicine 2007;11(5):1149–61. [PubMed: 17979890]

42. Lee TH, Seng S, Li H, Kennel SJ, Avraham HK, Avraham S. Integrin regulation by vascular endothelial growth factor in human brain microvascular endothelial cells: role of alpha6beta1 integrin in angiogenesis. J Biol Chem 2006;281(52):40450–60. [PubMed: 17085437]
43. Landowski TH, Gard J, Pond E, Pond GD, Nagle RB, Geffre CP, et al. Targeting integrin alpha6 stimulates curative-type bone metastasis lesions in a xenograft model. Mol Cancer Ther 2014;13(6):1558–66. [PubMed: 24739392]
44. Wang H, La Russa M, Qi LS. CRISPR/Cas9 in Genome Editing and Beyond. Annual review of biochemistry 2016;85:227–64.
45. Harryman WL, Gard JMC, Pond KW, Simpson SJ, Heppner LH, Hernandez-Cortes D, et al. Targeting the Cohesive Cluster Phenotype in Chordoma via beta1 Integrin Increases Ionizing Radiation Efficacy. Neoplasia 2017;19(11):919–27. [PubMed: 28954241]
46. Goel HL, Sayeed A, Breen M, Zarif MJ, Garlick DS, Leav I, et al. beta1 integrins mediate resistance to ionizing radiation in vivo by inhibiting c-Jun amino terminal kinase 1. J Cell Physiol 2013;228(7):1601–9. [PubMed: 23359252]
47. Wedlich-Soldner R, Betz T. Self-organization: the fundament of cell biology. Philosophical transactions of the Royal Society of London Series B, Biological sciences 2018;373(1747).
48. Gov NS. Guided by curvature: shaping cells by coupling curved membrane proteins and cytoskeletal forces. Philosophical transactions of the Royal Society of London Series B, Biological sciences 2018;373(1747).
49. McGarvey TW, Kariko K, Barnathan ES, Thomas J, Malkowicz SB. The expression of urokinase-related genes in superficial and invasive transitional cell carcinoma. International journal of oncology 1998;12(1):175–80. [PubMed: 9454902]
50. Tanaga K, Bujo H, Zhu Y, Kanaki T, Hirayama S, Takahashi K, et al. LRP1B attenuates the migration of smooth muscle cells by reducing membrane localization of urokinase and PDGF receptors. Arteriosclerosis, thrombosis, and vascular biology 2004;24(8):1422–8.
51. Demetriou MC, Cress AE. Integrin clipping: a novel adhesion switch? Journal of cellular biochemistry 2004;91(1):26–35. [PubMed: 14689578]
52. Sulyok GA, Gibson C, Goodman SL, Holzemann G, Wiesner M, Kessler H. Solid-phase synthesis of a nonpeptide RGD mimetic library: new selective alphavbeta3 integrin antagonists. J Med Chem 2001;44(12):1938–50. [PubMed: 11384239]
53. Gritsenko PG, Friedl P. Adaptive adhesion systems mediate glioma cell invasion in complex environments. J Cell Sci 2018. doi: 10.1242/jcs.216382
54. Shen MW, Arbab M, Hsu JY, Worstell D, Culbertson SJ, Krabbe O, et al. Predictable and precise template-free CRISPR editing of pathogenic variants. Nature 2018;563(7733):646–51. [PubMed: 30405244]
55. Duperret EK, Trautz A, Stoltz R, Patel A, Wise MC, Perales-Puchalt A, et al. Synthetic DNA-Encoded Monoclonal Antibody Delivery of Anti-CTLA-4 Antibodies Induces Tumor Shrinkage In Vivo. Cancer Res 2018;78(22):6363–70. [PubMed: 30287678]

Statement of significance:

This study shows an innovative strategy to block prostate cancer metastasis and invasion in the muscle through gene editing of a specific α6 integrin extracellular region.

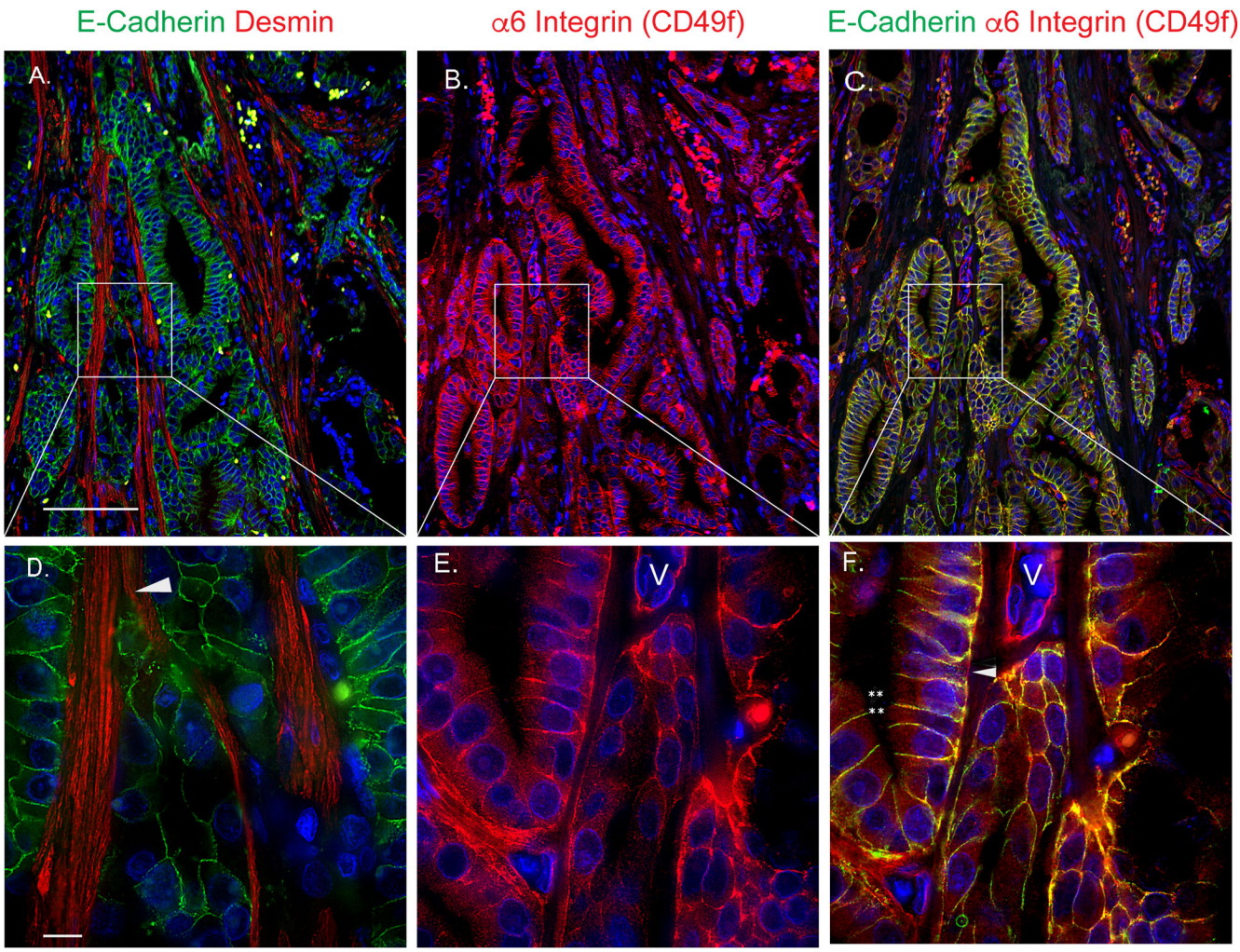

Figure 1.

Muscle invasive networks in human PCa express α6 integrin and E-cadherin. The same tissue section was stained for E-cadherin and desmin (Fig.1A) or α6 integrin alone (Fig.1B) or E-cadherin and α6 integrin (Fig.1C). Higher power images of same areas were collected for E-cadherin and desmin (Fig.1D) or α6 integrin alone (Fig.1E) or E-cadherin and α6 integrin (Fig.1F). Human PCa within radical prostatectomy de-identified specimens (**A, D**) was stained for E-cadherin (green), muscle (desmin, red) and nuclei (DNA, blue) or in (**B, E**) for α6 integrin (red) and nuclei (DNA, blue) or in (**C, F**) for E-cadherin (green), α6 integrin (red) and nuclei (DNA, blue). Tumor was invading between the smooth muscle (white arrow, **D**) between the muscle fibers and α6 integrin expressing vessel (V, **E**) was present as expected. Scale bar is 100 microns. Boxed areas in **A-C** are expanded in **D-F** with scale bar of 10 microns. Areas of α6 integrin and E-cadherin co-distribution in **F** (yellow), areas of cadherin only (green,**) and α6 integrin only (red, white triangle) were observed. Results are representative of at least 3 biological replicates (n=3) using either needle biopsy or radical prostatectomy de-identified specimens.

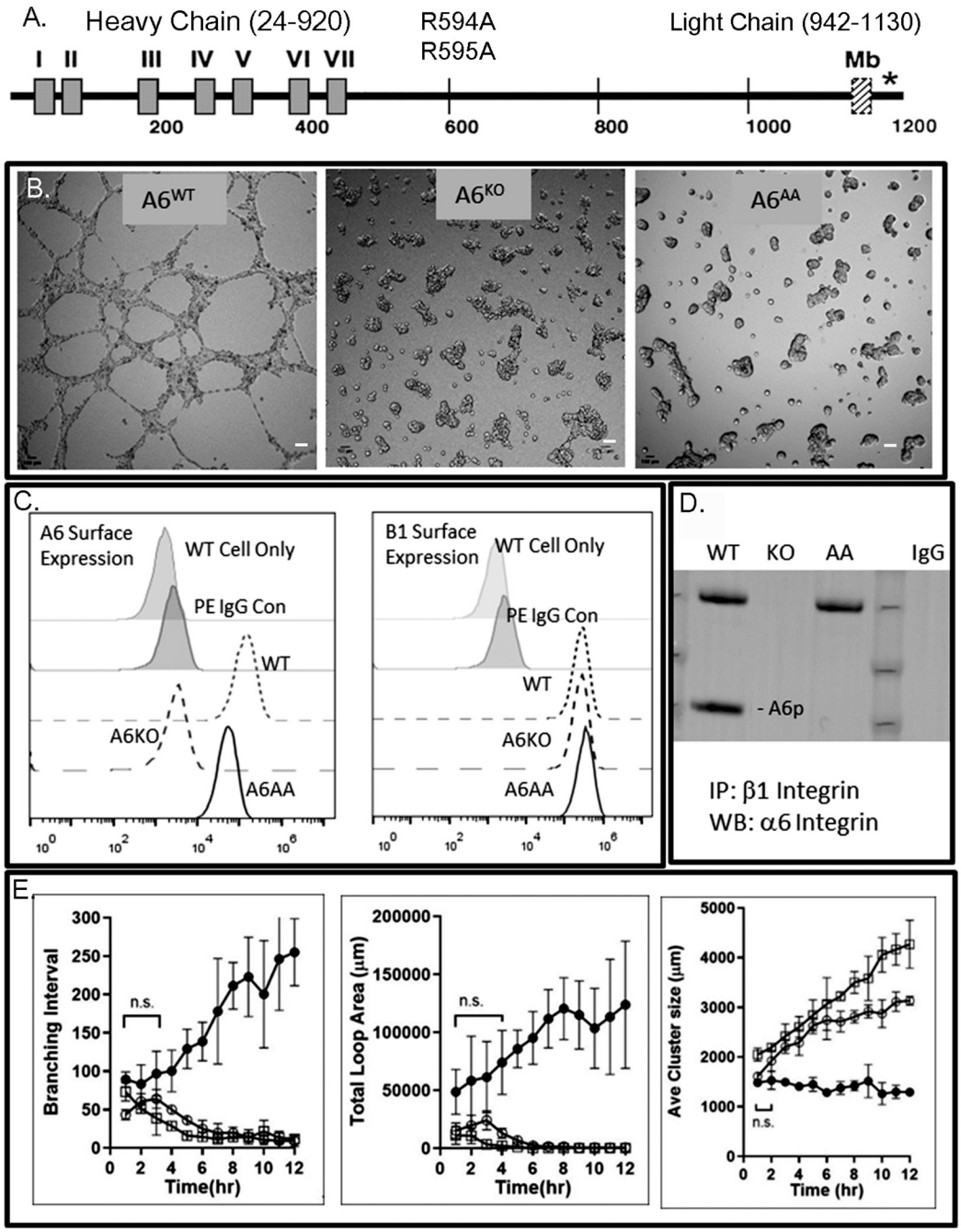

Figure 2.

Gene editing of α6 integrin prevents invasive networks and results in cohesive clusters. **A**. Schematic showing the amino terminal region of α6 integrin containing the extracellular repeated domains (I-VII) and the position of the R594A and R595A substitution mutations in the α6 integrin heavy chain (amino acids 24-920) and the domains of the light chain (amino acids 942-1130) containing the membrane spanning domain (Mb, striped box) and the cytoplasmic domain (*) at the carboxy terminus. **B**. DU145 α6WT (left), DU145 α6KO (center) and DU145 α6AA (right) networks at 12 hours on laminin containing Matrigel.

Scale bar: 500 microns. **C**. Flow cytometry profiles of α6 and β1 surface expression in all three cell lines. **D**. Immunoprecipitation (IP) of β1 integrin, followed by western blot (WB) detection of α6 and α6p (A6p) integrin. **E**. Network formation on laminin containing Matrigel during 12 hours of incubation using video microscopy. Networks (branching interval, total loop areas and cluster size) were measured using Image J software. Statistical significance was achieved between DU145 α6WT and DU145 α6KO cells and DU145 α6WT and DU145 α6AA cells at all time points unless otherwise indicated as not significant (n.s.) using an unpaired two-tailed student's t test where p value is < 0.05. Results are representative of at least 3 biological and technical replicates, n=12.

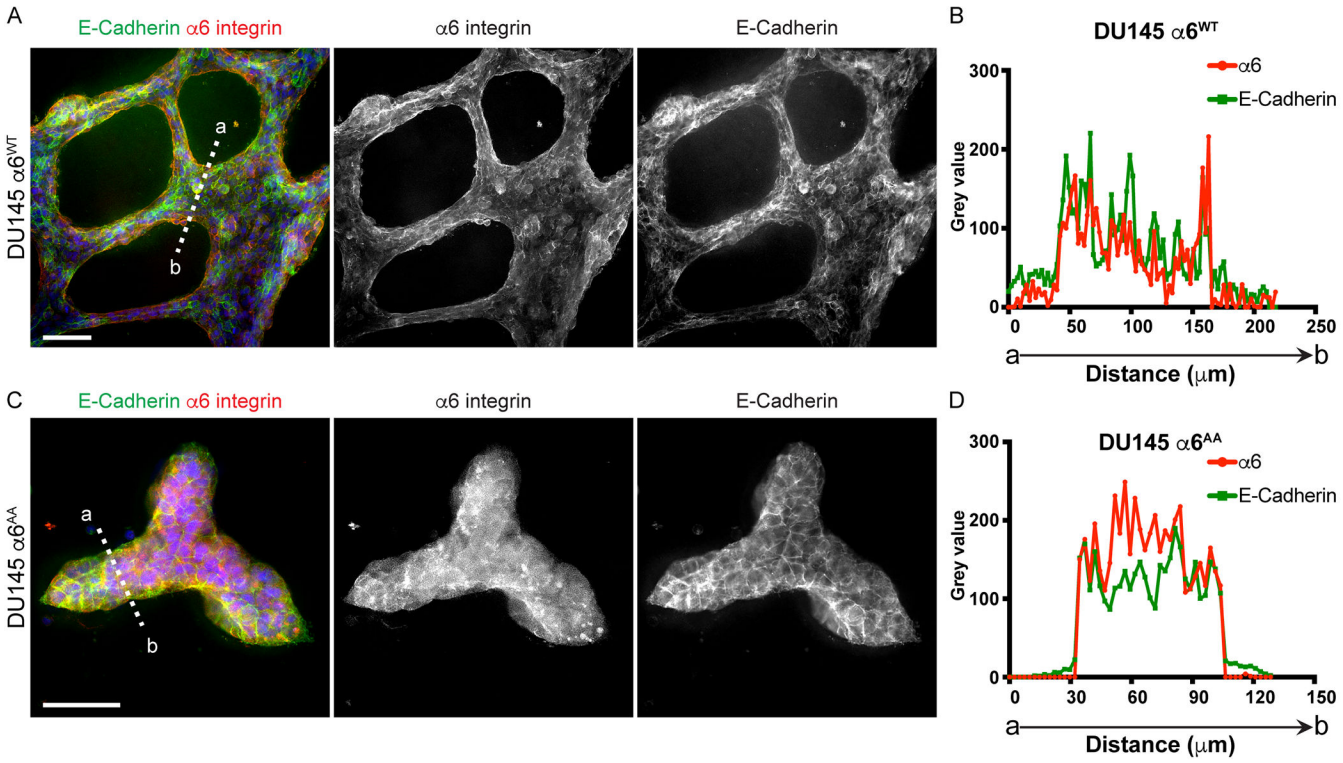

Figure 3.

The α6 integrin and E-cadherin distribute to a cell-cell location within invasive networks and cohesive clusters. The distribution of α6 integrin (red) and E-cadherin (green) in DU145 α6WT networks (**A, B**) or in DU145 α6AA cohesive clusters (**C, D**). The diagonal white lines on **A, C** are image lines from one side of the network (a) to the other side of the network (b), correspond to a distance of 200-300 microns and the pixel grey values are mapped (**B, D**). Results are representative of at least 3 independent experiments. Scale bars: 100 microns.

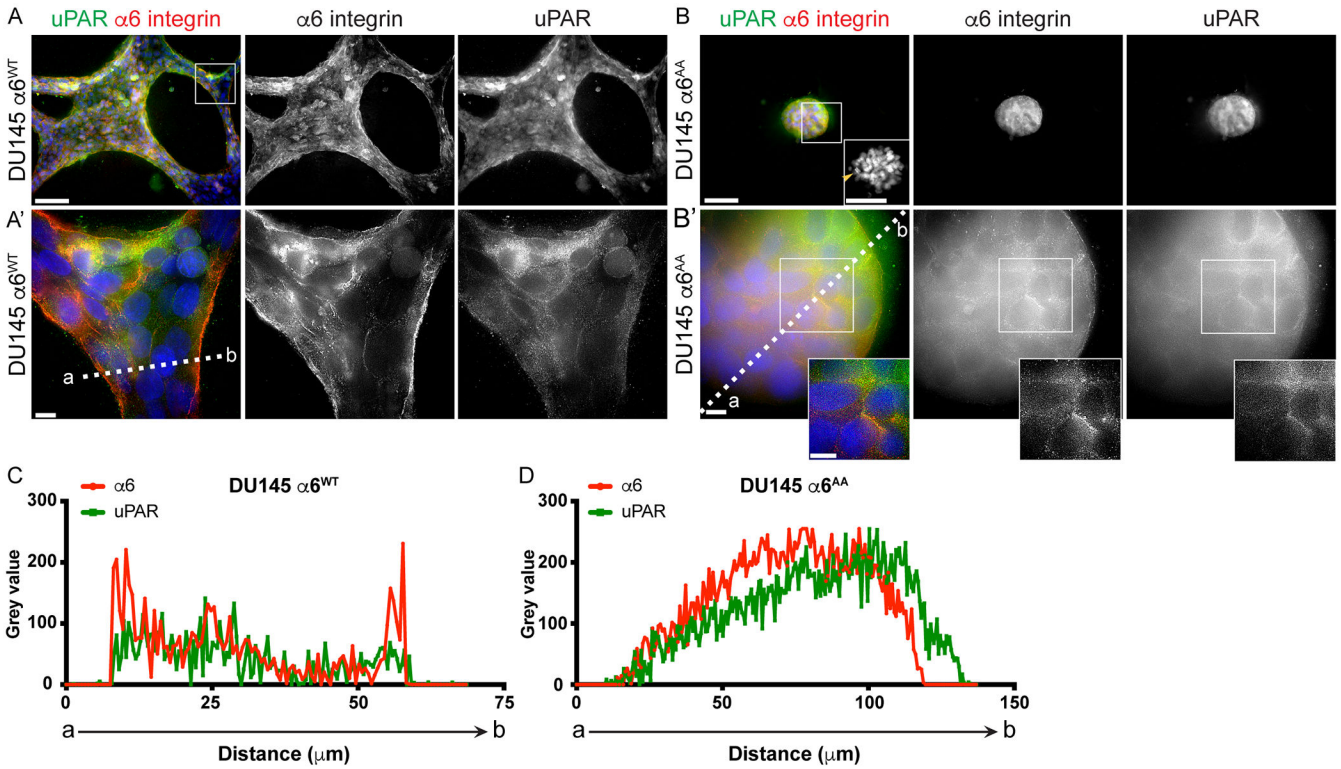

Figure 4.

Distribution of α6 integrin and uPAR in cell-cell and cell-ECM locations in networks and cohesive clusters. The distribution of uPAR (green) and α6 integrin (red) in DU145 α6WT networks (**A, A',C**) or in DU145 α6AA cohesive clusters (**B, B', D**). The cohesive clusters contain mitotic cells (**B**, inset, yellow arrow) and contain a cell-cell distribution of both uPAR and α6 integrin (**B'**). The diagonal white lines are the image lines used to map image signals. Results are representative of at least 3 independent experiments. Scale bars: 100 microns.

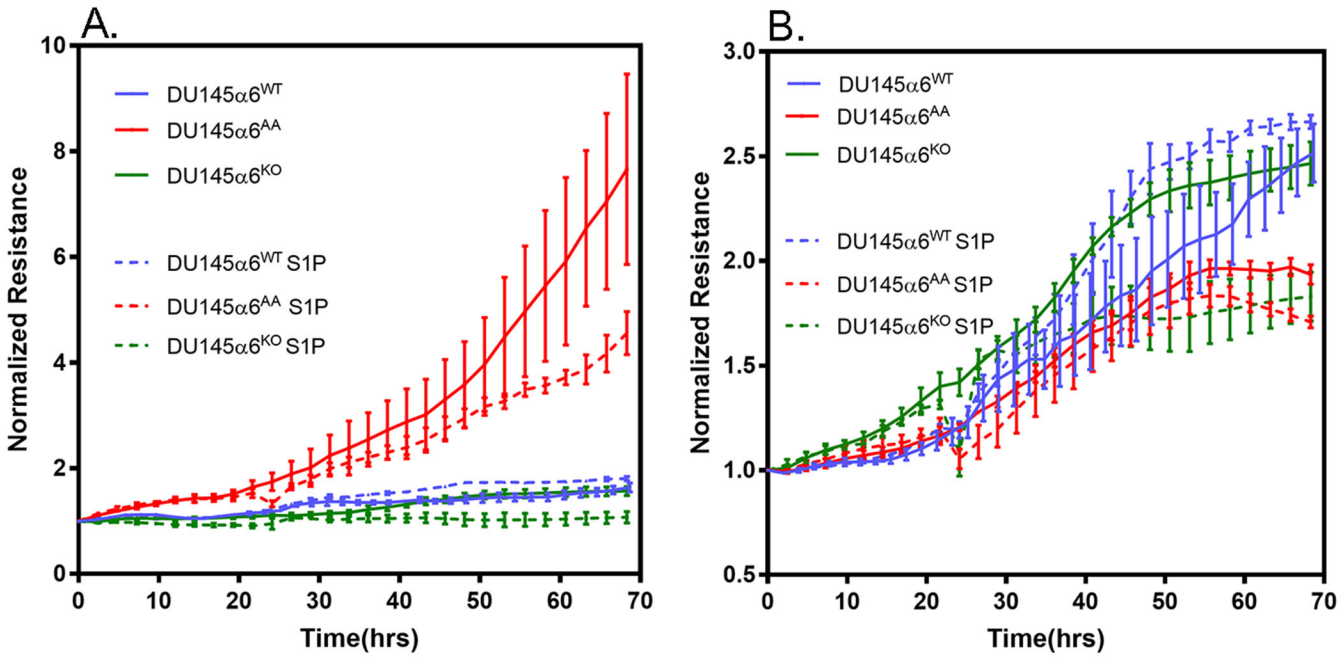

Figure 5.

Cell-Cell biophysical properties are increased in cells expressing the uncleavable α6 integrin mutant. **A**. Cell-Cell ECIS resistance measurements at 400 Hz in DU145 α6WT, DU145 α6KO and DU145 α6AA cells in the absence (solid lines) or presence (broken lines) of 1uM S1P treatment given at 24 hours after seeding. **B**. Cell-ECM Coverage by ECIS resistance measurements at 40,000 Hz in DU145 α6WT DU145 α6KO and DU145 α6AA cells in the absence (solid lines) or presence (broken lines) of 1uM S1P treatment given at 24 hours after seeding. Results are representative of at least 3 independent experiments.

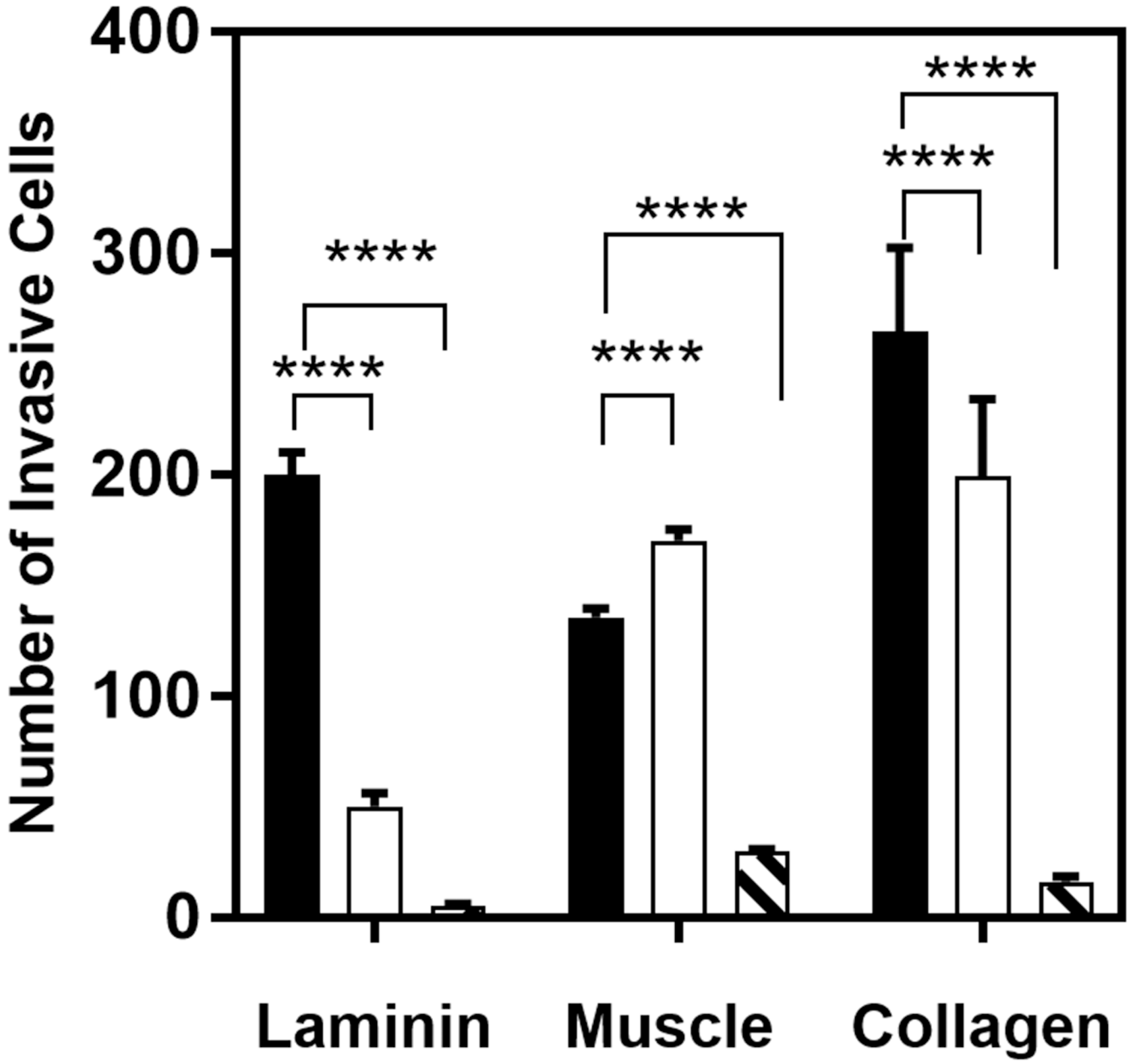

Figure 6.

Invasion is prevented by expression of uncleavable α6 integrin mutant (DU145 α6AA). Prostate tumor cells expressing the α6 integrin (DU145 α6WT solid bars) not expressing the α6 integrin (DU145 α6KO open bars) or a mutated and uncleavable α6 integrin (DU145 α6AA striped bars) were tested 16 hours later for their ability to invade through laminin containing Matrigel (laminin), a smooth muscle cell layer (muscle) or a collagen layer (collagen) using a modified Boyden chamber assay. The number of cells appearing on the underside of the insert were counted in triplicate wells. The standard error of the median values is shown and compared using a two-way ANOVA analysis (****$p<0.000001$).

Results are representative of at least 3 biological and technical replicates; n=364 for DU145 α6WT, n=370 for DU145 α6KO, and n=378 for DU145 α6AA.

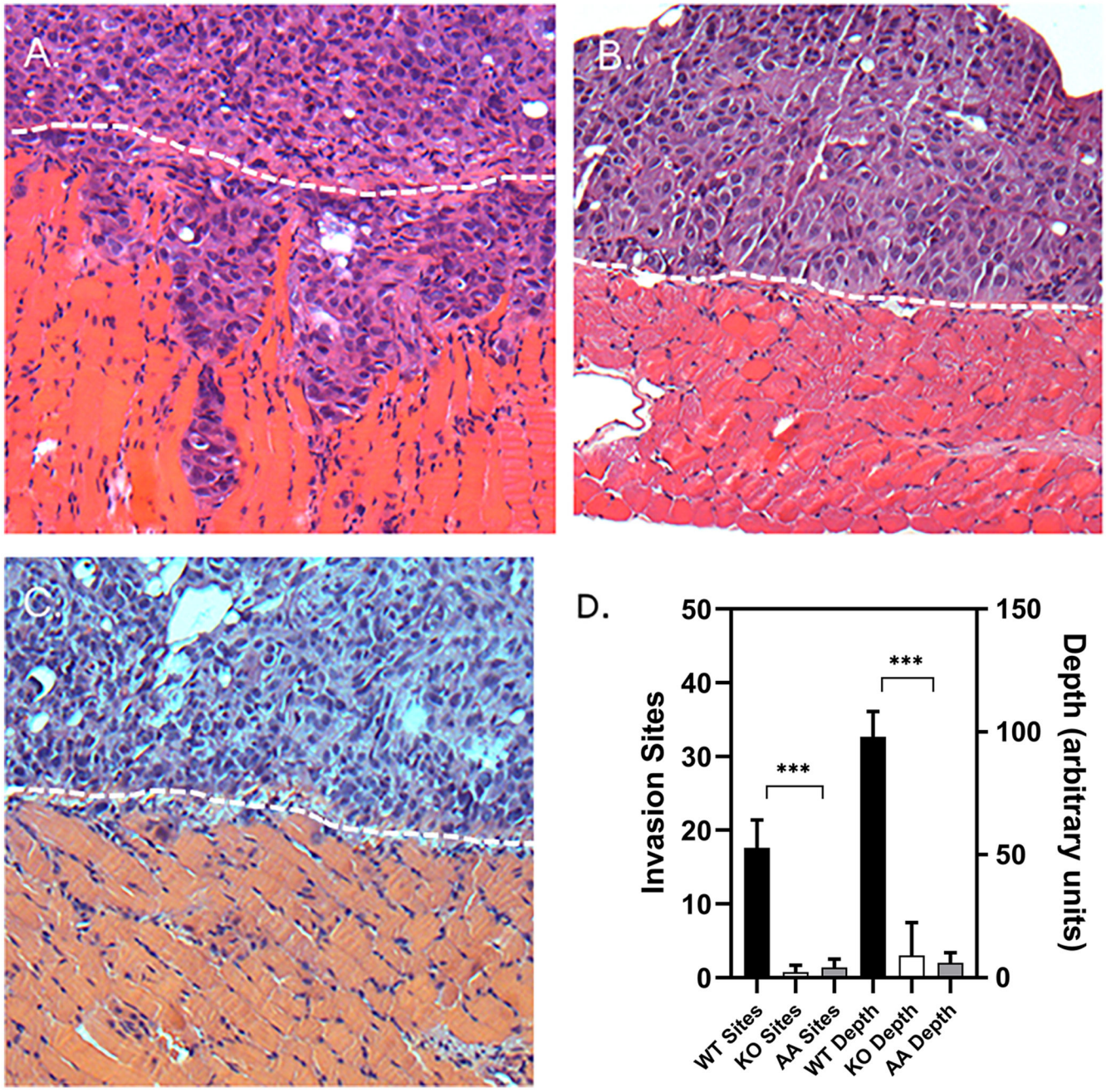

Figure 7.

Smooth muscle invasion is prevented by expression of uncleavable α6 integrin mutant (DU145 α6AA). Prostate tumor cells (1 x 10^7) expressing the α6 integrin (**A**, DU145 α6WT), not expressing the α6 integrin (**B**, DU145 α6KO) or a mutated and uncleavable α6 integrin (**C**, DU145 α6AA) were grown on the undersurface of the diaphragm in a mouse and harvested 8 weeks later. The resulting tissue sections are shown (**A**-**C**) stained with hematoxylin and eosin with the tumor (blue), the muscle surface (white dotted line), and the underlying muscle (pink). The number of invasion sites along a 4mm stretch of diaphragm and the maximum depth of invasion was measured using the images (**D**). The standard error

of the median values is shown and compared using a two-way ANOVA analysis (***$p<0.0001$). Results are representative of at least 4 biological and technical replicates, n=36.